Hydrogen-Induced Activation of the [NiFe]-Hydrogenase from *Allochromatium vinosum* as Studied by Stopped-Flow Infrared Spectroscopy[†]

Sergei Kurkin,[‡,#] Simon J. George,[§,#] Roger N. F. Thorneley,[§] and Simon P. J. Albracht*[,‡]

Swammerdam Institute for Life Sciences, Biochemistry, University of Amsterdam, Plantage Muidergracht 12, NL-1018 TV Amsterdam, The Netherlands, and Department of Biological Chemistry, John Innes Centre, Norwich Research Park, Colney, Norwich NR4 7UH, United Kingdom

Received January 20, 2004; Revised Manuscript Received March 26, 2004

ABSTRACT: The reaction between hydrogen and the [NiFe]-hydrogenase from *Allochromatium vinosum* in its inactive form has been studied by stopped-flow infrared spectroscopy. The data, for the first time, clearly show that at room temperature enzyme in the unready state, either oxidized or reduced, does not react with hydrogen. Enzyme in the ready state reacts with hydrogen after a lag phase of about six seconds, whereby a specific reduction of the enzyme occurs. The lag phase and the rate of reduction of the ready enzyme are neither dependent on the enzyme concentration nor on the substrate concentration, i.e., substoichiometric and 8-fold excess amounts of H_2 reduce the ready enzyme at the same rate. Oxygen delays this reaction but does not prevent it. The infrared changes lead us to suggest that the hydroxyl group, bridging between the Ni and the Fe atom in the active site, becomes protonated during this reduction. At physiological temperatures, this property of the inactive ready enzyme enables a full development of activity by substoichiometric H_2 concentrations.

Hydrogenases (reaction: $H_2 \leftrightarrow 2H^+ + 2e^-$) are among the oldest enzymes in nature and occur in a wide variety of microorganisms and some primitive eukaryotes (*1*). All hydrogenases contain transition metals. Three main classes can be distinguished. Two of them have been rather well characterized: (i) [Fe]-hydrogenases with Fe as the only metal; (ii) [NiFe]-hydrogenases, containing Ni, Fe, and Mg (*1*−*4*). The third class has long been thought to contain no metals at all (*5*, *6*), but was recently shown to contain an essential Fe atom (*7*).

This study focuses on the membrane-bound [NiFe]-hydrogenase from *Allochromatium vinosum*. Like the enzymes from *Desulfovibrio gigas*, *Desulfovibrio vulgaris* Miyazaki F, *Desulfovibrio fructosovorans*, *Desulfomicrobium baculatum*, and *Desulfovibrio desulfuricans*, for which the crystal structures have been solved (*8*−*16*), the *A. vinosum* enzyme belongs to the class of "standard" [NiFe]-hydrogenases. These enzymes consist of at least two subunits of about 60 and 30 kDa. The crystal structures revealed that the active site is a Ni−Fe center bound to the protein via thiols from four strictly conserved cysteine residues in the large subunit (Figure 1). There are three bridging ligands between Ni and Fe: two thiols and one nonprotein oxygen ligand, presumed to be an OH^- group. In addition to the two bridging thiols,

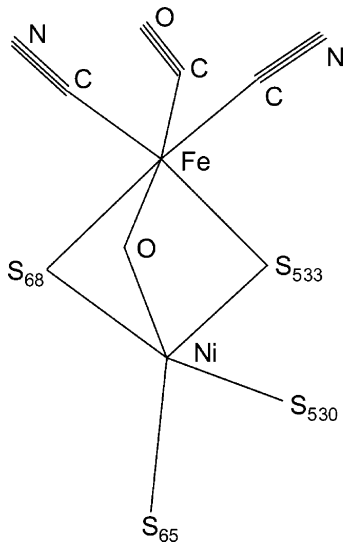

FIGURE 1: Structure of the active site of standard [NiFe]-hydrogenases based on the X-ray structure of the *D. gigas* enzyme (2frv (*9*)) and FTIR studies on the *A. vinosum* and *D. gigas* enzymes (*18*, *19*, *21*). In this representation, the bridging oxygen points toward the reader with the CO pointing in the opposite direction (see text for further details).

Fe is coordinated by three other nonprotein ligands which have been characterized by infrared spectroscopy (FTIR)[1] studies on the *A. vinosum* enzyme as two nonexchangeable CN^- groups and one nonexchangeable CO molecule (*17*−*19*). The FTIR spectra of most [NiFe]-hydrogenases are essentially identical (*20*, *21*). Hence, the active site is a $(RS)_2Ni(\mu\text{-}RS)_2(\mu\text{-}OH)Fe(CN)_2(CO)$ hetero-bimetallic center

[†] This work was supported by funds from the The Netherlands Organization for Scientific Research (NWO), Division for Chemical Sciences (CW) and by the UK Biotechnology and Biological Sciences Research Council, which also funded the development of the SF−FTIR apparatus used in these studies.

* To whom correspondence should be addressed: Phone: +31 20 5255130; fax: +31 20 5255124; e-mail: asiem@science.uva.nl.

[‡] University of Amsterdam.

[§] John Innes Centre.

[#] These authors contributed equally to this work.

[1] Abbreviations: FTIR, Fourier transform infrared spectroscopy; SF-FTIR, stopped-flow FTIR; BV, benzyl viologen; MV, methyl viologen.

10.1021/bi049854c CCC: $27.50
Published on Web 05/06/2004

(R = Cys). The small subunits of all [NiFe]-hydrogenases have a conserved cysteine motif, $CxxCx_nGxCxxxGx_mGCPP$ (n = 61 to 106, m = 24 to 61 (*3*)), that binds one [4Fe-4S] cluster. This cluster is located 14 Å from the Ni−Fe active site and is called the "proximal" cluster. Many hydrogenases contain two additional Fe−S clusters located in the small subunit which together with the proximal cluster form an almost linear array for facile electron transfer (*8*, *9*). Like the *D. gigas* enzyme, the *A. vinosum* enzyme contains one [3Fe-4S] cluster and two cubane clusters (*22*). The 3Fe cluster lies between the two cubane clusters and is called the "medial" cluster. The second cubane cluster is the "distal" cluster and has one edge exposed to solvent at the surface of the protein.

Traditionally, EPR has been used to monitor the redox changes of the Ni and the Fe−S clusters in the enzyme (for a review see ref *3*). Since the discovery of the CN^- and CO ligands in the *A. vinosum* enzyme by infrared spectroscopy (*17*, *18*), this technique has greatly contributed to the further understanding of the properties of the active site, not least because it enables EPR-silent states to be studied. It is now generally accepted that redox changes in the Ni−Fe site occur close to (or at) the Ni site (*23*, *24*). The low-spin Fe(II) ion, which was first observed (but not recognized as belonging to the active site) in Mössbauer spectra of the H_2-reduced *A. vinosum* enzyme (*22*), does not undergo a redox or spin state change when the enzyme is oxidized or reduced (*25*).

When purified aerobically, [NiFe]-hydrogenases are inactive. However, they can be activated by incubation with H_2. In this paper, we report the kinetics of the reaction of the *A. vinosum* hydrogenase in the inactive ready and unready states with H_2 and with mixtures of H_2 and CO or O_2. The recently developed technique of stopped-flow Fourier transform infrared spectroscopy (SF-FTIR) (*26*−*28*) has been used for the first time with any hydrogenase system to continuously monitor infrared changes starting ca. 60 ms after initiating the reaction.

EXPERIMENTAL PROCEDURES

Enzyme Purification and Sample Preparation. The growth of *A. vinosum* (strain DSM 185) and the solubilization, purification, and activity measurements of the membrane-bound hydrogenase were performed as described previously (*29*). The preparation used in this and the accompanying paper in this issue (*30*) had a specific H_2−BV activity of 300 U/mg (pH 8, 30 °C). The quality of the preparations was also checked by SDS−PAGE and by comparing the protein concentration (*31*) with the concentration determined by double integration of the EPR signals of the nickel or the $[3Fe\text{-}4S]^+$ cluster in the oxidized enzyme. Enzyme was dissolved in 50 mM Tris-HCl buffer (pH 8.0), concentrated (80−90 μM), and stored at −80 °C. This enzyme preparation and buffer were used throughout unless otherwise stated.

Enzyme mainly in the Ni_r* state was obtained by first reducing the enzyme under 1 bar H_2 for 30 min at 50 °C in a septum-capped bottle. Subsequently, the enzyme was reoxidized at 0 °C by quickly replacing the atmosphere in the bottle with 1 bar O_2 by evacuation and flushing. To prepare enzyme mainly in the Ni_u* state, the enzyme was first rebuffered in 50 mM MOPS buffer (pH 6.3) by repeated concentration and dilution (at least 20 times) in a Millipore Centricon YM-10 centrifugal filter unit. The enzyme was then incubated for 30 min at 50 °C under 1 bar H_2. Subsequently, the atmosphere in the bottle was replaced with 1 bar CO and the enzyme was then reoxidized at room temperature by the slow admittance of air via a thin needle though the septum. These methods are based on published procedures (*32*). Preparations containing a mixture of the Ni_r* and Ni_u* states were obtained in the same way as the Ni_r* samples, but with air replacing pure O_2. For every set of experiments, a freshly thawed batch of enzyme was converted into the required state. This meant that experiments performed on different days, although qualitatively reproducible, could not be compared on a precise quantitative basis, since the procedures described above to prepare the different states always gave slightly different ratios of ready and unready enzyme.

The various concentrations of H_2, CO, or O_2 and their mixtures were obtained by diluting gas-saturated buffer with an anaerobic buffer (flushed with oxygen-free N_2) or by mixing H_2, CO, and air-saturated buffer using Gastight Hamilton syringes. Dilutions were done in syringes without a headspace to avoid equilibration with a gas phase. Syringe plungers were moved slowly to avoid the generation of partial vacuums and any consequent outgassing.

SF-FTIR Measurements and Data Analysis. Infrared measurements were performed with a modified Bruker IFS66/S spectrometer (Bruker UK Ltd., Coventry, UK) equipped with an MCT detector cooled with liquid nitrogen. The stopped-flow circuit and cell were home-built as described previously (*26*, *27*, *33*). The drive system and stopped-flow cell were entirely contained within an anaerobic, dry glovebox (<2 ppm O_2; Belle Technology, Portesham, Dorset, UK) (*27*). The sample cell temperature was maintained at 25 °C for all experiments by means of a water-cooled jacket and thermostated circulation system. The path length of the IR cell was 48 μm. The data were collected from 2200 to 1700 cm^{-1} using a narrow band-pass filter located in front of the MCT detector to improve the signal-to-noise level. All spectra were measured with a resolution of 4 cm^{-1} with symmetric interferograms and a mirror velocity of 160 kHz. With the enzyme concentrations used, these settings gave the best compromise between noise and collection time on our instrument. The time resolution for these settings was 60 ms (i.e., the time to collect one spectrum). The reaction time of the first spectrum, collected after the flow stops, is 100 ± 20 ms. This spectrum and sometimes the second spectrum (160 ± 20 ms) showed background absorption offset effects related to relaxation of small cell deformations that occur during the flow phase. This phenomenon did not preclude the analysis of these spectra since these offsets are readily subtracted. All reaction times in this paper have an uncertainty of ± 20 ms. It is possible to obtain spectra at times as short as 18 ms with a precision of about 2 ms with our SF-FTIR apparatus (*34*). This was considered inappropriate for these experiments since, at this time resolution, spectroscopic signal-to-noise and wavenumber resolution are compromised. During the SF-FTIR experiments, the enzyme syringe (syringe 1) contained hydrogenase preconditioned as described in the text. The reactant syringe (syringe 2) contained the standard buffer (50 mM Tris-HCl, pH 8.0) with the additions specified in the text. Both syringes were of equal size, and their

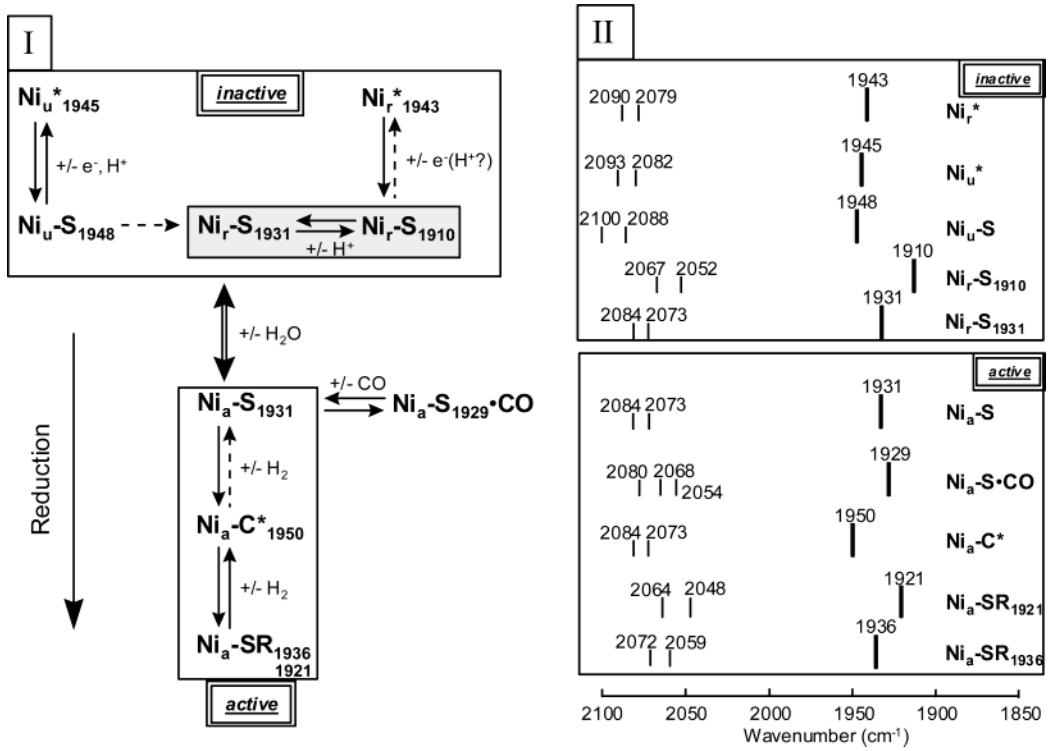

FIGURE 2: Schematic overview of the different (redox) states of the [NiFe]-hydrogenase from *A. vinosum*. (I) The states are those observed in redox titrations. The subscripts u, r, and a stand for unready, ready, and active, respectively. States marked with an asterisk (*) show a S = 1/2 EPR signal due to nickel. EPR-silent states have an S added; SR stands for silent reduced. The number added to each state as a subscript represents the stretching frequency of the intrinsic CO bound to Fe. The upper block shows states of inactive enzyme. The lower block shows the states of the active enzyme. *Note that the Ni_u-S, Ni_r-S, and Ni_a-S states are isopotential.* Dashed arrows represent very slow reactions (periods of hours). (II) Infrared bands arising from the active site are represented as stick spectra. All of the states except two have infrared bands assigned to $\nu(CN)_{sym}$, $\nu(CN)_{asym}$, and $\nu(CO)$ stretching vibrations. The $\nu(CN)$ bands are above 2000 cm^{-1} (thin lines), while the $\nu(CO)$ bands are below 2000 cm^{-1} (thick lines), except for the 2054 cm^{-1} band from extraneous CO bound to nickel. The Ni_r-S_{1931} and Ni_a-S states have the same set of infrared bands and can only be distinguished by their activity or by their reactions with CO. Enzyme reduced with 1 bar H_2 exists mainly in two Ni_a-SR states. The Ni_a-SR_{1936}/Ni_a-SR_{1921} ratio increases at lower pH values. Frequencies are taken from ref *41*, as obtained at 2 cm^{-1} resolution. Peak positions observed in the present study may differ slightly due to the resolution used (4 cm^{-1}).

contents were mixed in a 1:1 (v/v) ratio. Data were analyzed using the Bruker OPUS−NT software package and home-written customized fitting programs (George, S. J., unpublished observations).

EPR Measurements. EPR spectra and integrations measured in the Amsterdam laboratory were obtained as described previously (*35*). Enzyme samples prepared for SF-FTIR measurements were routinely characterized in the Norwich laboratory using an X-band Bruker 200D EPR spectrometer interfaced with to an ESP 1600 computer and fitted with an Oxford Instruments ERS900 liquid helium cooled flow cryostat.

RESULTS AND DISCUSSION

Rationale behind the Experimental Design. To facilitate the understanding of the experimental design and execution in this and the accompanying paper (*30*), a short overview of the present knowledge of the multiple states of the *A. vinosum* enzyme follows. A schematic representation of the states, together with their IR characteristics, is given in Figure 2.

Most [NiFe]-hydrogenases are purified aerobically in an oxidized, inactive state. X-ray structures show that this state has an extra bridging, nonprotein ligand between Ni and Fe in the active site (Figure 1). This is an oxygen species in the *D. gigas* enzyme (*8*, *9*), but a sulfur species in the enzyme from *D. vulgaris* Miyazaki (*11*). Two different oxidized states of the *A. vinosum* and *D. gigas* enzymes were initially identified by EPR. They both exhibit signals from Ni in the 3+ oxidation state. The two states are called "ready" (Ni_r*) and "unready" (Ni_u*) on the basis of their differential rates of activation by hydrogen as monitored by lag phases in activity assays using low-potential electron acceptors. The ready state shows a hydrogen-uptake activity within minutes, while the unready state requires hours (*36*−*38*). A proton-hyperfine splitting observed in the g_z line of the EPR spectrum of the ready, but not of the unready enzyme from *A. vinosum* suggested that the OH^- ligand is probably located in a different position in each state (*32*). It was therefore speculated that in the ready enzyme the OH^- group was no longer in a bridging position between Ni and Fe. However, recent X-ray structures of *D. fructosovorans* [NiFe]-hydrogenase in the Ni_r* state showed the presence of a bridging, nonprotein species (presumably oxygen; Volbeda, A., Martin, L., Cavazza, C., Matho, M., Faber, B. W., Roseboom, W., Albracht, S. P. J., Garcin, E., Rousset, M., and Fontecilla-Camps, J. C., unpublished experiments).

The Ni^{3+} in the ready and unready states can be reduced to an EPR-silent Ni^{2+} form; the corresponding states are termed Ni_r-S and Ni_u-S, respectively. In redox titrations in

the presence of mediating redox dyes, the Ni_u* to Ni_u-S conversion is a reversible $n = 1$ reaction (*39*, *40*). The reversibility persists at 2 °C (*29*). The pH dependence of the midpoint potential of the Ni_u*/Ni_u-S couple indicates that the single electron transfer is accompanied by a single proton transfer. The Ni_r* to Ni_r-S conversion is also a $n = 1$ reaction, but the involvement of a proton has not been shown. Curiously, this conversion is not reversible at 2 °C (*29*). It requires an elevated temperature (30 °C) to behave as a normal reversible redox transition. Infrared studies suggest that there are two forms of the Ni_r-S state that differ in their protonation state (*41*).

The response of the IR band arising from the indigenous CO of the Ni−Fe center to reduction with redox dyes is quite different for ready and unready enzyme. For the unready state (Ni_u*), the 1945 cm^{-1} band shifts to 1948 cm^{-1} upon reduction to the Ni_u-S state. Reduction of ready enzyme at 2 °C shifts the υ(CO) band from 1943 cm^{-1} (Ni_r*) to 1910 cm^{-1} (at pH 9; here called the Ni_r-S_{1910} state) or 1931 cm^{-1} (at pH 6; termed the Ni_r-S_{1931} state) (*41*). For the Ni_r-S state prepared at pH 6 and 2 °C, it has been found that the Ni−Fe distance is 2.60 Å, which is 0.25 Å shorter than the Ni−Fe distance in oxidized enzyme (*24*). The coordination number of the nickel decreases from five in the Ni_r* state to four in the Ni_r-S state (at low pH). Furthermore, the oxygen ligand could not be detected in the Ni-EXAFS spectra of this Ni_r-S state.

At room temperature the Ni_u-S state converts very slowly to the Ni_r-S state (*29*, *42*). In the *A. vinosum* enzyme, the Ni_u* and Ni_r* states cannot interconvert without reduction. All of these states (Ni_u*, Ni_r*, Ni_u-S, and the two Ni_r-S states) display no enzymic activity (*43*).

Under reducing conditions and at physiological temperatures (i.e., 25−30 °C for *A. vinosum*), standard [NiFe]-hydrogenases can be activated (minutes to hours). X-ray diffraction studies showed that in the reduced active enzymes the bridging O or S species is absent, while the Ni−Fe distance is ca. 0.25 Å shorter than that in the oxidized enzyme (*12*, *13*). As remarked above, EXAFS studies with the *A. vinosum* enzyme indicated that the removal of the O bridge and the shortening of the Ni−Fe distance from 2.85 to 2.60 Å has already occurred at the level of the Ni_r-S state prepared at 2 °C and pH 6.0 (the Ni_r-S_{1931} state) (*24*). However, this state is not yet active (*43*). Hence, our working hypothesis is that the OH^- bridge in the Ni_r* state is still present in the Ni_r-S_{1910} state, but becomes protonated at low pH leading to the Ni_r-S_{1931} state with the resulting water molecule not coordinated to the nickel. At 2 °C, the water molecule remains captured in the active-site pocket and sterically hinders the reaction with H_2. At room temperature, however, we assume that this water molecule is released thereby allowing the enzyme to convert into an active state without any change in its IR spectrum (the Ni_a-S_{1931} state; Figure 2).

The Ni−Fe site in active enzyme can exist in three different redox states (Figure 2). The most oxidized state is designated as Ni_a-S, the most reduced state as Ni_a-SR (which can exist in two pH-dependent substates) and an intermediate state as Ni_a-C*. Only the Ni_a-C* state shows an EPR signal from the Ni−Fe site ($S = 1/2$ system, indicated by the asterisks). The Ni_a-S to Ni_a-C* transition is induced by very low concentrations of hydrogen (0.01 bar); the reverse reaction is extremely slow (days) (*44*−*46*). The reaction is reversible in the presence of redox mediators (*47*). There is evidence that Ni−Fe site in the Ni_a-C* state contains a hydride in a position bridging between Ni and Fe (*1*, *48*, *49*). When the hydrogen concentration is increased the Ni_a-C* state converts into the EPR-silent Ni_a-SR state. The reaction Ni_a-C* + $H_2 \leftrightarrow Ni_a$-SR is the *only equilibrium reaction* of hydrogen with the enzyme in the absence of redox mediators (*45*).

Excess CO converts active enzyme into an inactive EPR-silent state (Ni_a-S·CO). The added carbon monoxide binds to the actives site, as inferred from FTIR studies (*42*). X-ray diffraction studies showed that the added CO binds to nickel opposite to the bridging thiol provided by the last Cys residue in the C-terminus of the large subunit (S_{533} in Figure 1) (*15*). All these states have different infrared spectra (Figure 2). A more detailed description of the properties of active enzyme can be found in the accompanying paper (*30*).

Reaction of Hydrogen with Enzyme in the Ni_u State at pH 6.3.* Enzyme (90% in the Ni_u* state as determined by EPR) was mixed with H_2-saturated buffer. As indicated in panel I of Figure 3, the first two spectra with valid data (spectra two and three, representing the time lapses 60−120 and 120−180 ms) had a higher background absorbance due to slight pressure-induced deformations of the IR cell after mixing. Since in all time-dependent changes a reference wavelength was used, these two spectra were included in our analyses. The three-dimensional representation of the data further shows only one υ(CO) band at the start of the reaction (at 1945 cm^{-1}) and two small υ(CN) bands (at 2093 and 2082 cm^{-1}). These three bands belong to the Ni_u* state (Figure 2). It can be clearly observed in this plot that after a lag phase during which essentially no spectral changes occurred, the υ(CO) band shifted to a higher frequency (1948 cm^{-1}). At the same time, changes in the υ(CN) region were detected. Important here is the appearance of a band at 2100 cm^{-1}, which is characteristic for the Ni_u-S state (Figure 2). Two very faint bands at 1936 and 1921 cm^{-1}, associated with the Ni_a-SR states, also appeared and increased very slowly in amplitude.

The kinetics of the changes at 1945 and 1948 cm^{-1}, with the absorbance at 1963 cm^{-1} as an internal reference, are plotted in panel II of Figure 3. It can be seen that the lag phase is ca. 120 s. Over the next 100 s, a slow disappearance of the 1945 cm^{-1} band occurred and simultaneously, the strong υ(CO) band at 1948 cm^{-1} appeared. These changes were complete at 250 s. It is obvious from this figure that the Ni_u* state does not rapidly react with H_2. Once the Ni_u-S state was formed (at 250 s), a subsequent very slow decrease of the 1948 cm^{-1} band (Figure 3II, trace B) occurred. Hence, also the Ni_u-S state does not react rapidly with H_2.

As will be shown later, enzyme in the Ni_r* state can react with H_2 within seconds and then becomes active. We therefore interpret the events in Figure 3 at this point as follows. The small amount of ready enzyme in the preparation (10%) is responsible for the reaction with H_2. Slow intermolecular electron transfer from this portion of reduced active enzyme to oxidized unready enzyme subsequently results in the reduction of the latter to the Ni_u-S state (1948 cm^{-1} band). It is known for the *A. vinosum* enzyme that under reducing conditions the Ni_u-S state can very slowly

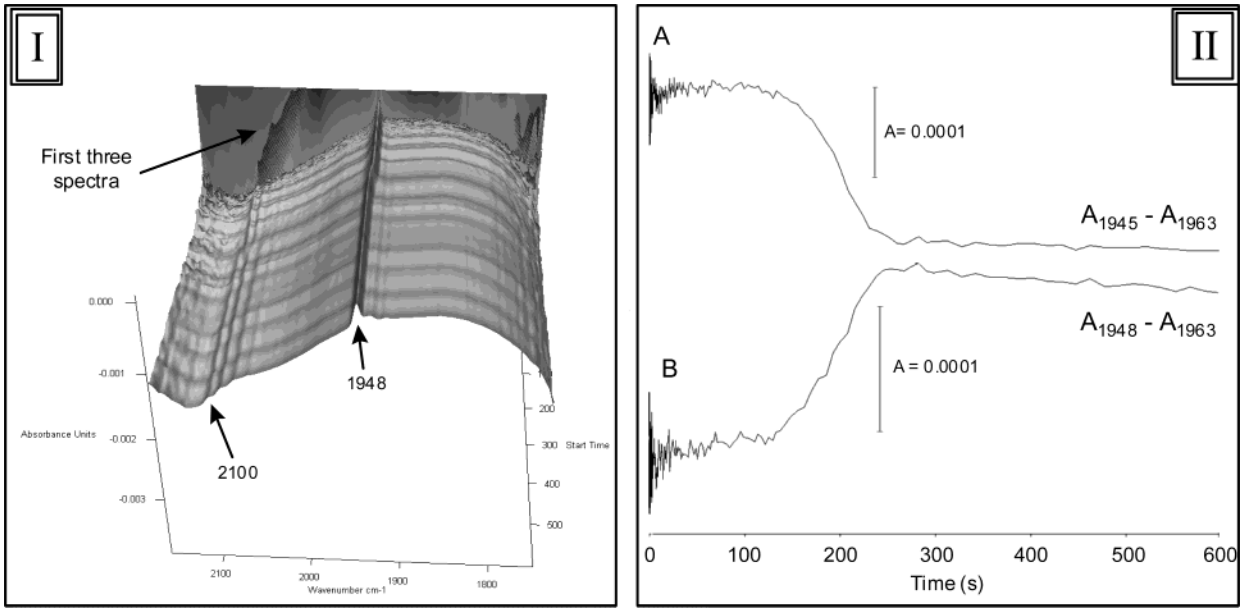

FIGURE 3: The reaction of H_2 with enzyme in the Ni_u* state at pH 6.3. Syringe 1 contained enzyme that was 90% in the Ni_u* state and 10% in the Ni_r* state (in 50 mM MOPS buffer, pH 6.3). Syringe 2 contained the same buffer saturated with H_2 (800 μM). Panel I: Three-dimensional representation of the spectral changes occurring during 10 min after mixing (1:1, v/v). The time axis (0−600 s) runs from back to front, the absorbance axis (0.004 units) runs from bottom to top, while the wavelength axis runs from 2150 cm^{-1} (left) to 1850 cm^{-1} (right). The arrows indicate key features in the spectra. The first spectrum is not reliable. The second and third spectra have a background shift due to slight deformations of the infrared cell that occur immediately after mixing. Panel II: Time-dependence of the amplitudes of the 1945 (A) and 1948 cm^{-1} (B) bands. The absorbance at 1963 cm^{-1} was taken as a reference.

(hours) convert into the Ni_r-S state (*29*, *42*). The same has been shown for the *D. gigas* enzyme (*21*). This explains the very slow decrease of the 1948 cm^{-1} band (between 250 and 600 s). Once formed, the Ni_r-S state converts into active enzyme, which then reacts with H_2 (Figure 2) forming mainly the Ni_a-SR states (1936/1921 cm^{-1} bands). It is concluded at this point that both the Ni_u* and Ni_u-S states do not readily react with H_2. However, the data do not exclude a slow (minutes) reaction. Before investigating this reaction in more detail, it is necessary to describe the kinetic properties of enzyme in the ready state.

Reaction between H_2 and Enzyme in the Ni_r State. (a) Effect of Different Hydrogen Concentrations.* The *A. vinosum* enzyme can be converted to 95% or more into the Ni_r* state by full activation with H_2 at pH 9.0 followed by subsequent oxidation of the enzyme by a quick dilution into oxygen-saturated buffer (*32*). We obtained concentrated enzyme preparations (80 μM) with 95% of the enzyme in the Ni_r* state, as determined by EPR, following essentially the same procedure used at pH 8 (outlined in Experimental Procedures). Enzyme in this state was mixed with H_2-saturated buffer (800 μM). The observed changes were now much faster and the lag phase was much shorter than in the previous experiment. The changes at 1943 (disappearance of the Ni_r* state), 1950 (appearance of the Ni_a-C* state), and 1936 cm^{-1} (appearance of the Ni_a-SR state) are shown in Figure 4I. The final spectrum did not show any of the 2100 cm^{-1} band arising from the Ni_u-S state (Figure 4IV, trace A). After a lag phase of about 6 s (at 25 °C and with 40 μM enzyme), the ready state disappeared (decrease of the 1943 cm^{-1} band). The development of the bands at 1950 cm^{-1} (Ni_a-C*) and 1936/1921 cm^{-1} (Ni_a-SR) showed that a mixture of active enzyme states was produced simultaneously.

The same type of experiment was performed with progressively lower hydrogen concentrations i.e., 200, 100, 50, 25, and 12.5 μM H_2 (concentrations after mixing). The lag phase preceding the decrease of the 1943 cm^{-1} band did not noticeably change and was about 6 s at all hydrogen concentrations. The time courses for the reactions with 25 and 12.5 μM H_2 are shown in Figure 4II,III. The lag phases (7 and 6 s, respectively) and $t_{1/2}$ times (9 s in both cases) were the same within error. There was a remarkable transient appearance of a 1950 cm^{-1} band (Ni_a-C*), peaking at 17 s, during the disappearance of the 1943 cm^{-1} band (Figure 4II, trace B and III, trace C). Instead of the 1936/1921 cm^{-1} band, now a single band appeared at 1931 cm^{-1} (lag phases 11 and 16 s, $t_{1/2}$ times 12 and 11 s with 25 and 12.5 μM H_2, respectively). Although these hydrogen concentrations are lower than that of the enzyme (40 μM), the lag phase and the initial rate of decrease of the 1943 cm^{-1} band were the same as those observed with higher H_2 concentrations. The only difference was that the rate toward the end of the reaction slightly diminished (see arrow in Figure 4III, trace A). This suggests that under the present conditions the ready enzyme has a high affinity for H_2 and can still react with hydrogen concentrations about 20-fold lower than that of the enzyme.

A clear difference between the experiments with the different hydrogen concentrations was the final redox state of the enzyme (Figure 4IV). At the higher concentrations (100 to 400 μM H_2), an equilibrium mixture of the Ni_a-SR (1936/1921 cm^{-1} bands) and Ni_a-C* (1950 cm^{-1}) states was obtained. The final spectra obtained with substoichiometric H_2 concentrations (25 and 12.5 μM) looked very different. The main band was at 1931 cm^{-1} and is due to the Ni_a-S/Ni_r-S_{1931} states. Small bands were observed at 1910 cm^{-1} (Ni_r-S_{1910} state), 1950 cm^{-1} (Ni_a-C* state), or 1943 cm^{-1}

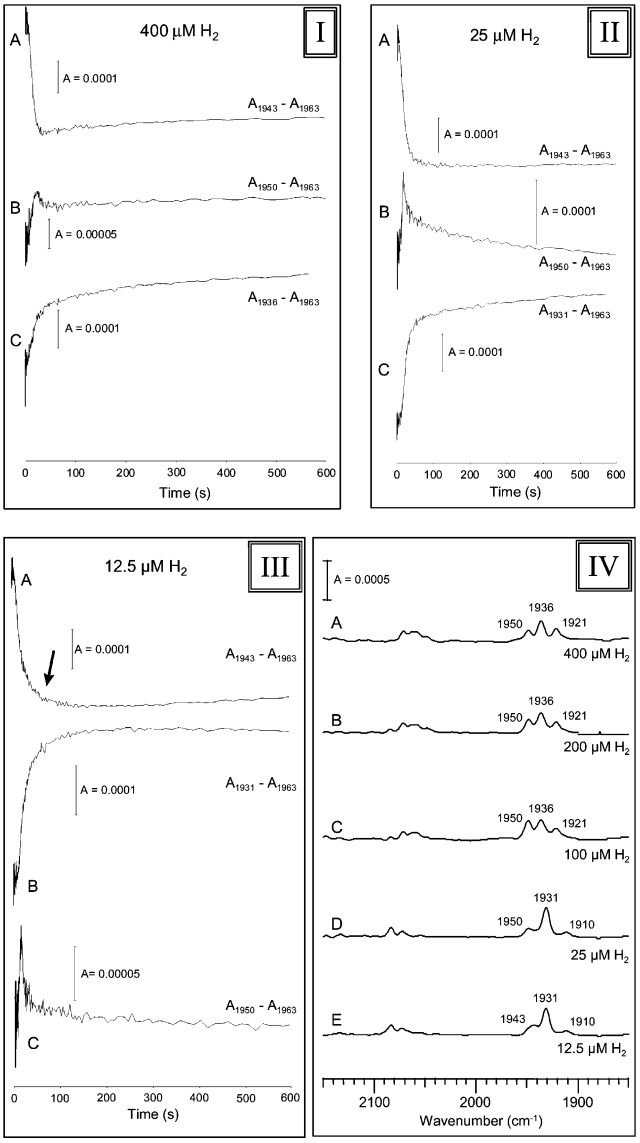

FIGURE 4: The reaction of enzyme in the Ni_r* state with different concentrations of H_2. Syringe 1 contained enzyme that was 95% in the Ni_r* state and 5% in the Ni_u* state (pH 8). Syringe 2 was filled with buffer containing different hydrogen concentrations. The panels I to III show the time-dependent changes of selected IR bands (as indicated; 1963 cm^{-1} absorbance as reference) after mixing with buffer containing 800 μM H_2 (I), 50 μM H_2 (II), and 25 μM H_2 (III). Panel IV shows the infrared spectra obtained 10 min after mixing with five different hydrogen concentrations (concentrations after mixing as indicated). The spectra in this and the following figures were baseline corrected.

(Ni_r* state). For an explanation of these results, it is useful to introduce the following short-hand notations for the various enzyme species since in addition to the Ni−Fe center ($n = 1$ redox component), the Fe−S clusters ($n = 1$) will also undergo redox changes in the reaction with H_2 ($n = 2$). The ready state can be written as $Fe^{2+}(OH^-)Ni^{3+}\cdot P^{2+}M^+D^{2+}$ where OH^- stands for the bridging oxygen species, P^{2+} for the oxidized proximal $[4Fe\text{-}4S]^{2+}$ cluster, M^+ for the oxidized medial $[3Fe\text{-}4S]^+$ cluster and D^{2+} for the oxidized distal $[4Fe\text{-}4S]^{2+}$ cluster. We will also refer to this state as Ni_r*(ooo), where "o" stands for an oxidized Fe−S cluster (order: proximal, medial, distal). With 12.5 and 25 μM H_2, concentrations significantly less than that of the enzyme (40 μM), the data are consistent with the following sequence of events.

Initially, H_2 reacts with the Ni_r* state to form the Ni_r-S_{1931} state as written in eqs 1 and 2:

$$Fe^{2+}(OH^-)Ni^{3+}\cdot P^{2+}M^+D^{2+} + H_2 \rightarrow Fe^{2+}(H_2O)Ni^{3+}(H^-)\cdot P^{2+}M^+D^{2+} \quad (1)$$

$$Fe^{2+}(H_2O)Ni^{3+}(H^-)\cdot P^{2+}M^+D^{2+} \rightarrow Fe^{2+}(H_2O)Ni^{2+}\cdot P^{2+}M^0D^{2+} + H^+ \quad (2)$$

Because the active site Fe is six coordinate in the inactive enzyme, and the Ni is five coordinate, the activation of H_2 is most likely to occur at the vacant coordination site on the Ni (see Figure 1). We suggest that the bridging hydroxyl group becomes protonated and in this particular reaction acts as the base to promote the heterolytic cleavage of the H_2 molecule on Ni in the Ni_r* state. The Ni-bound hydride in the transient state is then oxidized resulting in the one electron reduction of both the 3Fe cluster and the Ni (the two centers with the highest redox potential). The proton in eq *2* can either be released or used for local charge compensation. The overall reaction can also be written as eq 3, where "r" stands for a reduced Fe−S cluster:

$$Ni_r\text{*(ooo)} + H_2 \rightarrow Ni_r\text{-}S_{1931}\text{(oro)} + H^+ \quad (3)$$

As mentioned before the Ni−Fe distance decreases from 2.85 Å in the Ni_r* state to 2.60 Å in the Ni_r-S_{1931} state, so a structural rearrangement of the active site takes place. In view of the high redox potential of the 3Fe cluster (−10 mV at pH 8), the reaction in eq 3 is essentially irreversible. We note that in [NiFe]-hydrogenases containing only the proximal cluster such as the NAD^+-reducing enzyme from *Ralstonia eutropha* (*3*, *50*) an activation of inactive enzyme by H_2 must proceed in a different way. Also in enzymes that have a cubane cluster instead of the 3Fe cluster, the reductive activation by H_2 may proceed differently, since the redox potential of the cubane cluster is much lower than that of the 3Fe cluster.

At 25 °C, the water molecule in the Ni_r-S_{1931} state is proposed to be released within a few tenths of a second from the active-site pocket producing the Ni_a-S state (eq 4).

$$Ni_r\text{-}S_{1931}\text{(oro)} \rightarrow Ni_a\text{-}S_{1931}\text{(oro)} + H_2O \quad (4)$$

Recent kinetic electrochemical studies with the *A. vinosum* enzyme are in agreement with such a reaction (*51*). The Ni_a-S_{1931}(oro) state has a very high affinity for H_2. When no oxidants are present hydrogen binds essentially irreversibly as a hydride in a fast reaction (ms time scale) to form the Ni_a-C* state. During this reaction, the Ni is oxidized and an electron is initially transferred to the proximal cluster as in eq 5.

$$Fe^{2+}\text{-}Ni^{2+}\cdot P^{2+}M^0D^{2+} + H_2 \rightarrow Fe^{2+}(H^-)Ni^{3+}\cdot P^+M^0D^{2+} + H^+ \quad (5)$$

Since the redox potential of the distal cluster is higher than that of the proximal cluster (*40*), the electron is rapidly passed on to the distal cluster (eq 6).

$$Fe^{2+}(H^-)Ni^{3+}\cdot P^+M^0D^{2+} \rightarrow Fe^{2+}(H^-)Ni^{3+}\cdot P^{2+}M^0D^+ \quad (6)$$

With excess H_2 this Ni_a-C*(orr) state reacts with yet another (third) H_2 molecule in a reversible reaction to form the Ni_a-SR states (eq 7).

$$Fe^{2+}(H^-)Ni^{3+}\cdot P^{2+}M^0D^+ + H_2 \rightarrow Fe^{2+}(H^-)Ni^{2+}\cdot P^+M^0D^+ + 2H^+ \quad (7)$$

The reactions of active enzyme are studied and discussed in detail in the accompanying paper (*30*).

With (sub-)stoichiometric H_2 concentrations, not all of the ready enzyme can react in this way. Once activated by one hydrogen molecule, the enzyme can very rapidly and tightly bind a second hydrogen to form the stable Ni_a-C* state, and so all of the hydrogen will be consumed by only part of the enzyme molecules. The remaining oxidized enzyme is subsequently reduced via (slower) intermolecular electron transfer by the reduced distal [4Fe-4S] cluster in enzyme that has reacted with H_2. The data of Figure 4II,III show that the reducing equivalents from the bound hydride in the Ni_a-C* state are also redistributed, since the increase of the 1950 cm^{-1} band was only a transient one. After the redox equilibration with substoichiometric amounts of H_2 (12.5 and 25 μM), the final products are a mixture of oxidized enzyme (Ni_r* state; 1943 cm^{-1}), enzyme in the Ni_r-S_{1931}/Ni_a-S states (the major part; we cannot distinguish between these two states by infrared spectroscopy), enzyme in the Ni_a-C* state (1950 cm^{-1}) and a small amount of the Ni_r-S_{1910} state (which is proposed to have an OH^- bridge present). This result (Figure 4IV, traces D and E) is in qualitative agreement with the expectations. In fact, the spectra show that the degree of reduction is a little higher than expected, possibly due to an overestimation of the enzyme concentration and/or an underestimation of the hydrogen concentration.

(b) Effect of Varying the Ready Enzyme Concentration on the Reaction with Hydrogen. In this set of experiments, the hydrogen concentration was kept constant (400 μM after mixing). An enzyme preparation with at least 90% in the Ni_r* state was used at final mixed concentrations of 40, 20, and 10 μM. The changes observed at 1943 cm^{-1} are shown in Figure 5. The lag times and kinetics of the 1943 cm^{-1} decrease were comparable at all three enzyme concentrations (lag phases 6, 7, and 11 s, $t_{1/2}$ times 9, 9, and 9 s for 40, 20, and 10 μM enzyme). This is consistent with hydrogen reacting directly with the active site in the ready enzyme and without any further intermolecular enzyme reactions occurring.

Since the lag phase and the *initial* rate of the reaction did not depend on the enzyme concentration or on the H_2 concentration, we conclude that under these conditions both of these parameters may be determined by rate-limiting intramolecular reactions occurring after formation of the E−H_2 complex (eq 8).

$$E + S \rightarrow ES \rightarrow EP \quad (8)$$

We hypothesize that these intramolecular reactions are associated with the rearrangement in the active site on going from the Ni_r*(ooo) state (Ni−Fe distance 2.85 Å) to the Ni_r-S_{1931}(oro) state (Ni−Fe distance 2.60 Å). Figure 4 showed that with very low H_2 concentrations (e.g., 12.5 μM) the rate of the reaction slowed (see arrow in Figure 4III, trace A) during the *last phase* of the reaction (where the H_2 concentration becomes less than ca. 5% of the enzyme concentration). Under those conditions, the formation of ES (eq 8) became rate limiting.

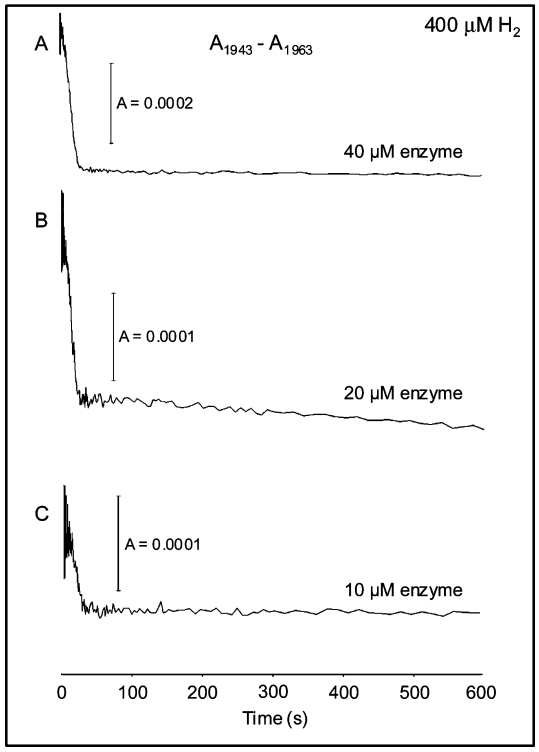

FIGURE 5: Reaction of different concentrations of ready enzyme with H_2. Syringe 1 contained enzyme that was 90% in the Ni_r* state (pH 8). Syringe 2 contained buffer saturated with H_2 (800 μM). The three traces show the time-dependent changes of the 1943 cm^{-1} band for 40 μM (A), 20 μM (B), and 10 μM (C) enzyme (final concentrations). The 1963 cm^{-1} absorbance was used as the reference.

(c) Effect of the Presence of O_2 on the Reaction of Ready Enzyme with H_2. The short lag phase in the reaction of the ready enzyme with hydrogen and its independence of either the H_2 concentration or the enzyme concentration could have been due to the presence of residual oxygen in the enzyme preparation. However, if this were the case, the rate of oxygen consumption by the enzyme would have been expected to be dependent on the enzyme concentration. To further investigate this, anaerobic ready enzyme was mixed with buffer containing known concentrations of both hydrogen and oxygen. The control experiment with only H_2 (200 μM after mixing) is shown in Figure 6, trace A.

When 25 μM oxygen was also present the reaction proceeded with essentially the same time course (Figure 6, trace B). However, on increasing the oxygen concentration to 62.5 μM, the lag phase was clearly extended and the rate of decrease of the 1943 cm^{-1} band diminished noticeably (Figure 6, trace C). The lag phase in the absence of oxygen (7 s) was nearly the same as that in the presence of 25 μM O_2. It increased to 20 s with 62.5 μM O_2 (Figure 6). The half times of the 1943 decrease were 10, 12, and 28 s, respectively. The experiment shows that oxygen does not prevent the reaction between hydrogen and the ready enzyme, but merely delays it. When oxygen was absent, the final hydrogen concentration after completion of the reaction is about 200 μM minus the amount of H_2 consumed by the enzyme during the reaction. When 62.5 μM O_2 was present,

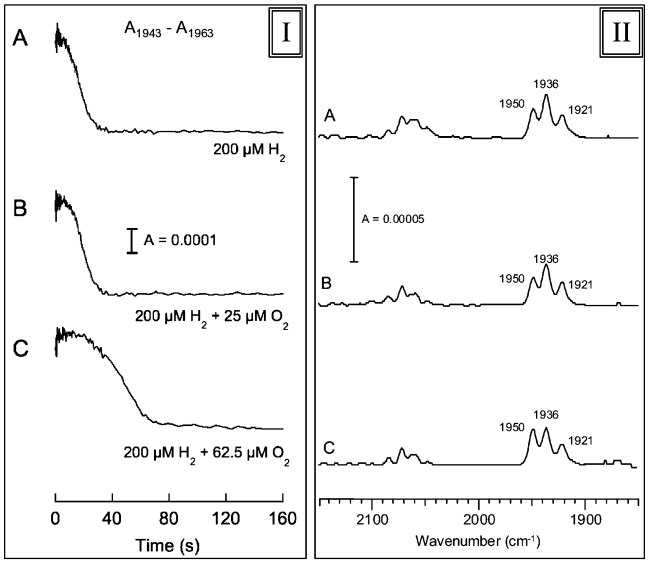

FIGURE 6: The effect of oxygen on the reaction of enzyme in the Ni_r* state with hydrogen. Syringe 1 contained enzyme that was 95% in the Ni_r* state (pH 8). Syringe 2 was filled with buffer containing: 400 μM H_2 (traces A; the spectrum in panel II, trace A is the same as the spectrum in Figure 4IV, B), 400 μM H_2 + 50 μM O_2 (traces B), or 400 μM H_2 + 125 μM O_2 (traces C). The concentrations after mixing are given in the figure. The spectra in panel II were obtained 10 min after mixing.

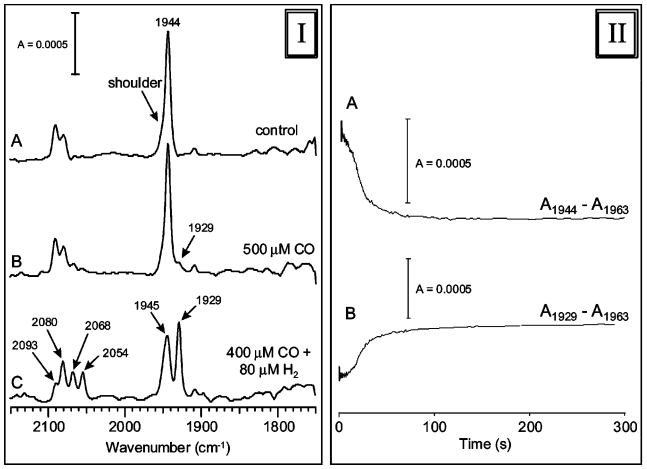

FIGURE 7: Reaction of a mixture of ready (46%) and unready (54%) enzyme with H_2 in the presence of carbon monoxide. Syringe 1 contained enzyme (pH 8). Panel I: (A) Control; spectrum 3 min after mixing with anaerobic buffer; (B) control; spectrum 10 min after mixing with buffer containing 1000 μM CO; (C) spectrum 10 min after mixing with buffer containing 160 μM H_2 and 800 μM CO. Panel II: time-dependent changes of the 1944 (A) and 1929 cm^{-1} (B) bands (absorbance at 1963 cm^{-1} as reference) during the reaction with H_2 plus CO resulting in spectrum C in panel I.

it is anticipated that the oxygen would consume 125 μM H_2, and so the reducing equivalents of 75 μM of H_2 would remain for equilibration with 40 μM enzyme. This final condition is comparable to that of the reaction with 100 μM H_2 in the absence of added oxygen (Figure 4). Indeed, the spectrum obtained after the reaction with 200 μM H_2 plus 62.5 μM O_2 (Figure 6II, trace C) is very similar to Figure 4.IV, trace C. However, it does differ from the spectrum obtained with 200 μM H_2 (Figure 6II, trace A); the latter spectrum clearly shows a higher degree of reduction (more Ni_a-SR (1936/1921 cm^{-1}) relative to Ni_a-C* (1950 cm^{-1})). This shows that the added oxygen in the experiment of Figure 6 is consumed. This important observation explains the delaying effect of oxygen displayed in the kinetic trace (longer lag phase, slower rate of decrease of the 1943 cm^{-1} band; Figure 6I, trace C). From this trace, the rate constant for oxygen consumption under these conditions is estimated to be about ca. 0.03 s^{-1}, which is 4 orders of magnitude slower than the rate of the H_2−BV reaction (470 s^{-1}).

Reactions of Enzyme Comprising Mixtures of the Ni_r and Ni_u* States.*

(a) Reaction with Hydrogen in the Presence of CO. Carbon monoxide is a strong inhibitor of the enzyme. Since it only binds to active enzyme, this property can be used to trap active enzyme in the Ni_a-S·CO state. Thus, when a mixture of ready and unready enzyme is reacted with H_2 in the presence of CO, within seconds the ready enzyme should be trapped in the inactive Ni_a-C·CO state allowing the reaction of H_2 with the Ni_u* state to be studied without any interference from the ready enzyme.

Figure 7I, trace A shows a control spectrum in the absence of CO and H_2 (mixing with N_2-flushed buffer) with a υ(CO) band at 1944 $cm^{-1}$and a clear shoulder on the high-frequency side. The υ(CN) bands are not resolved. Both features are in agreement with the expected overlap of the spectra from the Ni_r* and Ni_u* states (see Figure 2). Spectrum B shows another control. Mixing the enzyme preparation with CO-saturated buffer did not affect the 1944 cm^{-1} band. A very faint band at 1929 cm^{-1} (<2% of the total υ(CO) band area) was observed, which may arise from a small amount of active enzyme or from a reaction with H_2 impurities in the CO gas.

When both H_2 (80 μM) and CO (400 μM) were present after mixing, the 1929 cm^{-1} band diagnostic of the Ni_a-S· CO state appeared (Figure 7I, trace C). The other bands characteristic of this state, two υ(CN) bands at 2080 and 2068 cm^{-1} plus a υ(CO) band at 2054 cm^{-1} from extraneous CO bound to Ni, can also be seen. In addition, clear bands characteristic of the Ni_u* state were identified (a CO band at 1945 cm^{-1} and a CN band at 2093 cm^{-1}). The appearance of the 1929 cm^{-1} band ($t_{1/2}$ = 24 s) accompanied the decrease of the 1944 cm^{-1} band ($t_{1/2}$ = 20 s) within error as shown in Figure 7II. We assign these changes to the reaction of ready enzyme with H_2 and the subsequent reaction of the resulting activated enzyme with CO. The product, enzyme in the Ni_a-S·CO state, cannot react with H_2, and so the reaction ceases with all of the H_2-activated ready enzyme trapped in this state. The 1945 cm^{-1} band in the final spectrum (Figure 7I, trace C) is responsible for the shoulder in the control spectrum (see arrow in trace A). The amplitude of this band did not change between 30 s and 10 min. As no 2100 cm^{-1} band could be detected, we assign it to enzyme in the Ni_u* state. This experiment, for the first time, directly demonstrates that enzyme in the unready state cannot react with H_2 at 25 °C.

(b) Reaction with Different H_2 Concentrations. When using 400 μM H_2 (after mixing), virtually no changes were observed over the first 43 s (Figure 8I, traces A−C and Figure 9, trace A). Subsequently, the 1944 cm^{-1} band, which is a composite of the 1943 cm^{-1} band from the Ni_r* state and the 1945 cm^{-1} band from the Ni_u* state, started to decrease in amplitude over the next ca. 30 s and then leveled off at about 75 s after initiating the reaction. Simultaneously, a band at 1948 cm^{-1} appeared (initially as a shoulder)

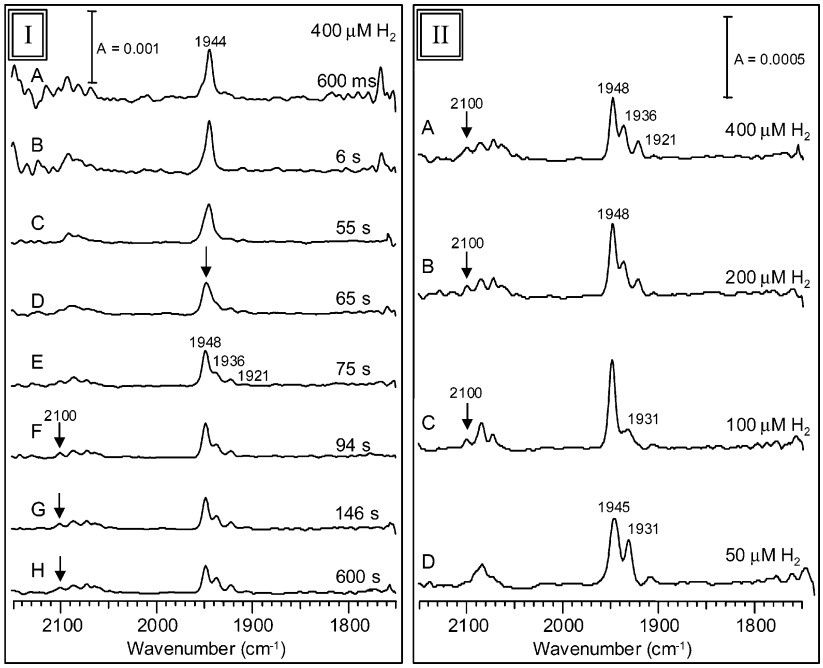

FIGURE 8: The reaction of a mixture of ready (35%) and unready (65%) enzyme with hydrogen. Syringe 1 was filled with enzyme (pH 8.0). Syringe 2 contained buffer with various hydrogen concentrations. Panel I: syringe 2 contained 800 μM H_2. After mixing, spectra A−H were obtained at the indicated times. Panel II: spectra obtained 10 min after mixing with buffer with different hydrogen concentrations (concentrations after mixing are indicated).

together with small bands at 1936 and 1921 cm^{-1}. The latter two bands are due to the Ni_a-SR states. The 1948 cm^{-1} band is mainly due to the Ni_u-S state since also a well-resolved band at 2100 cm^{-1} is observed (see arrows in Figure 8I, traces F−H). At longer times (Figure 8I, trace H), the 1948 cm^{-1} band (Ni_u-S) very slowly decreased with a simultaneous increase of the 1936/1921 cm^{-1} bands (Ni_a-SR). As previously shown by EPR studies (*45*), and in the accompanying paper by SF-FTIR (*30*), active enzyme in the presence of excess H_2 is mainly in the Ni_a-SR state. Only 10−15% remains in the Ni_a-C* state. In Figure 8I, traces D−G, up to half of the enzyme is in the Ni_a-SR state. It then follows that under 400 μM H_2, a small percentage of the enzyme (<5%) must be in the Ni_a-C* state with a υ(CO) band around 1950 cm^{-1}. This small band will be obscured by the more intense 1948 cm^{-1} band of the Ni_u-S state. Thus, between 1 and 10 min the spectrum represents a mixture of the Ni_u-S, Ni_a-C* and Ni_a-SR states.

These data can be compared with those shown in Figures 3 and 4, and the explanation is similar to that given there. After the lag phase, enzyme in the Ni_r* state is reduced to the Ni_r-S_{1931} state according to eq 3, activates to Ni_a-S (eq 4), binds H_2 to form the Ni_a-C* state (eqs 5 and 6) and subsequently reacts with a third H_2 molecule resulting in the formation of the Ni_a-SR states (eq 7). Reduced enzyme reacts with enzyme in the Ni_u* state, converting it to the Ni_u-S state. The subsequent extremely slow decrease of the 1944 cm^{-1} band (between 50 and 300 s in Figure 9, trace A) is due to the Ni_u-S to Ni_r-S conversion: the disappearance of the 1948 cm^{-1} band from Ni_u-S (Figure 8I, traces E−H) also influences the absorbance at 1944 cm^{-1} to a small extent. In turn, the Ni_r-S state reacts with H_2 to form an equilibrium mixture of the active states, causing the increase of the 1936/1921 cm^{-1} bands.

The effect of lower hydrogen concentrations (reaction of 200, 100, and 50 μM H_2 with 40 μM enzyme) was also investigated. The kinetics of the changes at 1944 cm^{-1} were the same as with 400 μM H_2 (Figure 9, traces B−D), but the reaction with all three hydrogen concentrations showed a shorter lag phase (about 22 s). The spectra obtained 10 min after mixing were diagnostic of a mixture of several states and depended on the hydrogen concentration (Figure 8II). At 400 and 200 μM H_2, the Ni_a-SR states (1936/1921 cm^{-1}) were clearly present, together with bands from the Ni_u-S state (υ(CO) at 1948 cm^{-1} and υ(CN) at 2100 cm^{-1}). As explained above, a small peak at 1950 cm^{-1} (Ni_a-C*) should also be present. With 100 μM H_2 bands from the Ni_a-SR state were absent. However, a small band at 1931 cm^{-1} (Ni_a-S/Ni_r-S_{1931} states) was seen. Bands from the Ni_u-S state were still prominently present. With 50 μM H_2 (and 40 μM enzyme, essentially stoichiometric) only two clear υ(CO) bands at 1945 and 1931 cm^{-1} were observed. The 1945 cm^{-1} band is assigned to unreacted enzyme in the Ni_u* state. It should be mentioned that during the reactions with 100 μM H_2 weak transient bands from the Ni_a-SR states were observed. With 50 μM H_2 no transient Ni_a-SR states appeared; instead only a weak transient band from the Ni_a-C* state was seen (data not shown). We tentatively conclude from this observation that the most effective reductant for enzyme in the Ni_u* state is probably an enzyme molecule in the Ni_a-SR state.

These experiments show that the length of the lag phase and the rate of the reaction of H_2 with a mixture of ready and unready enzyme is not dependent on the H_2 concentration over a 20-fold range (400 to 50 μM) down to a concentration close to stoichiometric with that of the enzyme (but see below). In experiments with several different, freshly prepared mixtures of ready and unready enzyme, we noticed that the duration of the lag phase varied with the preparation. Within a set of experiments with one preparation, however, the results obtained with different amounts of hydrogen were reproducible, i.e., the lag phase was independent of the

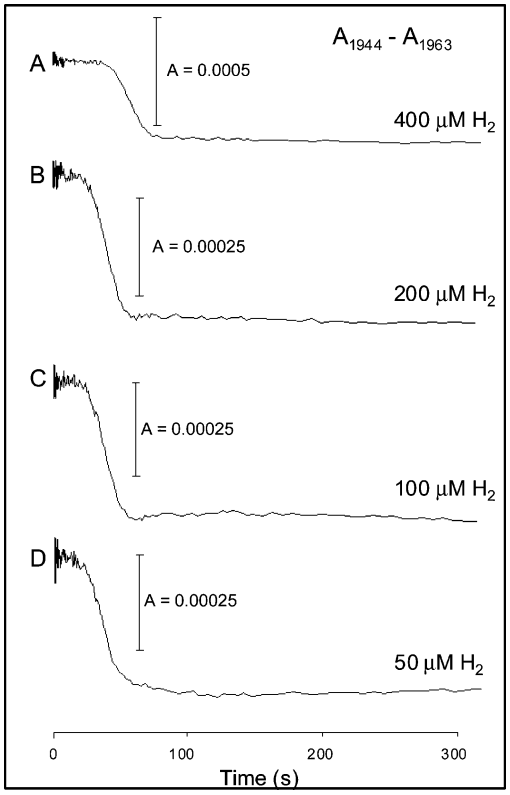

FIGURE 9: Time dependence of the decrease in amplitude of the 1944 cm^{-1} band in the experiment shown in Figure 8. The H_2 concentrations after mixing are indicated. The absorbance at 1963 cm^{-1} was used as a reference.

hydrogen concentration. However, we did notice that it was important to carefully remove all oxygen from the solutions before starting the experiments. Residual oxygen is probably the reason for the slightly longer lag phase in Figure 9, trace A, this being the first experiment in this series (see also Figure 6 for the effect of oxygen).

(c) Reactions of Hydrogen with a Mixture of Ready and Unready Enzyme at Different Enzyme Concentrations. A preparation containing 35% ready and 65% unready enzyme was used. The results obtained with three different enzyme concentrations are presented in Figure 10. As before, the 1944 cm^{-1} band decreased due to the disappearance of the 1943 cm^{-1} band from Ni_r* and the 1945 cm^{-1} band from Ni_u*. At the same time the Ni_u-S (1948 cm^{-1}) and Ni_a-SR (1936/1921 cm^{-1}) appeared. In this case, a pronounced dependence of the kinetics on the enzyme concentration was observed. Dilution of the enzyme increased the lag phase and decreased the rate at which the intensity of the 1944 cm^{-1} band was lost. In contrast to the reactions of ready enzyme with H_2, these results show that the overall reaction of hydrogen with a mixture of ready and unready enzyme is very dependent on the enzyme concentration. We do not fully understand these observations. After a lag phase, the ready enzyme in the mixture is activated by reactions with H_2. It then transfers electrons to unready enzyme in an intermolecular reaction. The rate of the overall process, i.e., the disappearance of the 1944 cm^{-1} band, clearly decreases on diluting the enzyme. The relative rates are estimated as 2.5, 1.6, and 1 for 40, 20, and 10 μM enzyme, respectively. The deviation from a second-order reaction (squared dependence on total enzyme concentration) can be explained by complex formation between the two enzyme forms. Such complexes

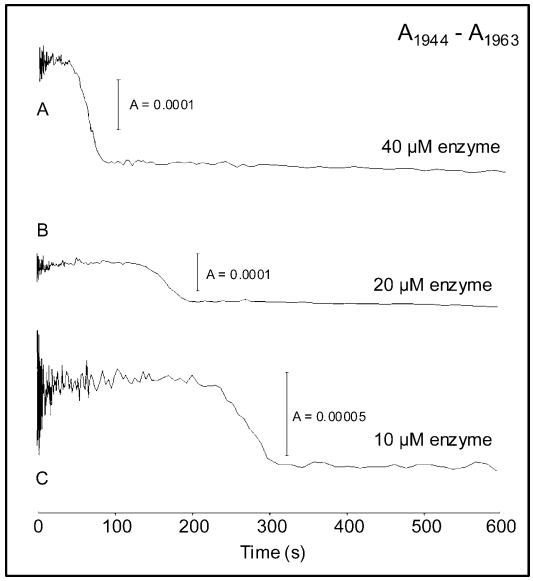

FIGURE 10: Effect of the enzyme concentration on the reaction of hydrogen with a mixture of ready (35%) and unready (65%) enzyme. Syringe 2 contained buffer with 800 μM H_2. Syringe 1 contained 80 μM (A), 40 μM (B), or 20 μM (C) enzyme (concentrations after mixing are indicated in the figure).

are not uncommon for solubilized membrane-bound enzymes. The relative changes in amplitude of the 1944 cm^{-1} band (expressed in absorption units) are 4, 2, and 1, which correlate well with the enzyme concentrations of 40, 20, and 10 μM, respectively. This and the fact that only one exponential phase is observed indicate that these amplitude changes represent the *simultaneous* disappearance of the Ni_r* (1943 cm^{-1}) and Ni_u* (1945 cm^{-1}) states. From a comparison with the data of enzyme mainly in the ready state (Figures 4 and 5), especially with respect to the lag phases, it can then be concluded that the ready enzyme molecules in the ready/unready mixture used in Figure 10 do not react with H_2 in an independent way, i.e., their behavior is dramatically influenced by the presence of unready enzyme molecules. We presently do not understand this. A more detailed kinetic analysis using a range of time-resolved spectroscopic techniques is beyond the scope of the present study but is clearly merited.

CONCLUSIONS

For clarity, the major conclusions of this study are summarized below and depicted in Figure 11.

(1) Enzyme in the unready state, either oxidized (Ni_u*) or reduced (Ni_u-S), does not react with H_2. The Ni_u* state can only be reduced via an intermolecular reaction with reduced active enzyme, or by reduced artificial electron donors. Under reducing conditions, the Ni_u-S state slowly (hours) converts to the Ni_r-S state, which subsequently activates. This is the only route for activation of unready enzyme.

(2) Enzyme in the Ni_r* state has high affinity for H_2. After a lag phase of about 6 s, the enzyme is reduced. The rate of reduction is the same with H_2 to enzyme concentration ratios of 10:1 to 1:20. The observations are consistent with the idea that the Ni_r* state is directly converted to the Ni_r-S_{1931} state in the initial reaction with hydrogen and that the bridging OH^- in the active Ni−Fe site may function as the base for the heterolytic cleavage of H_2 in this initial reaction. At 25

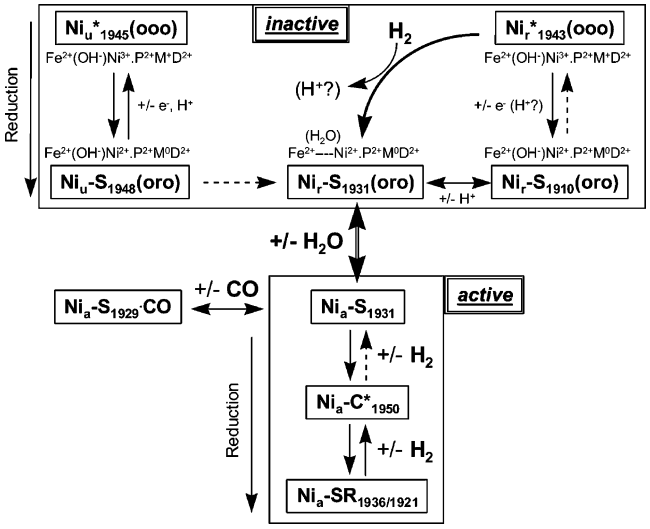

FIGURE 11: Schematic overview of the proposed reactions of the *A. vinosum* [NiFe]-hydrogenase with hydrogen. In addition to the short-hand notations used for the active site in Figure 2, also the status of the Fe−S clusters have been introduced for the inactive enzyme states. For example, the ready state can be written as $Fe^{2+}(OH^-)Ni^{3+}{\cdot}P^{2+}M^+D^{2+}$ where OH^- stands for the bridging oxygen species, P^{2+} for the oxidized proximal $[4Fe\text{-}4S]^{2+}$ cluster, M^+ for the oxidized medial $[3Fe\text{-}4S]^+$ cluster, and D^{2+} for the oxidized distal $[4Fe\text{-}4S]^{2+}$ cluster. We will also refer to this state as Ni_r*(ooo), where "o" stands for an oxidized Fe−S cluster (order: proximal, medial, distal). The only states that can react with H_2 are the Ni_r*, Ni_a-S, and Ni_a-C* states. The Ni_a-SR state can release H_2, but the Ni_r-S_{1931} state cannot. The Ni_u*/Ni_u-S and Ni_r*/Ni_r-S_{1910} redox transitions can only occur with electrons provided by redox dyes or by reduced, active enzyme via an intermolecular electron-transfer reaction. H_2 reacts directly with the Ni−Fe site of the Ni_r* state to give the Ni_r-S_{1931} state. It is proposed that during this reaction the bridging OH^- is protonated to water which is no longer bound to the Ni−Fe center, but remains in the active site pocket. This allows a decrease of the Ni−Fe distance from 2.85 to 2.60 Å. Activation is achieved by the loss of this water molecule from the active site pocket, which is proposed to be controlled by the temperature-dependent dynamics of the protein (i.e., water is retained at 2 °C, but lost at 25 °C).

°C the inactive Ni_r-S_{1931} state converts to the active Ni_a-S state within a few tenths of a second. These reactions are proposed to form the basis of the mechanism of activation of ready enzyme by H_2. It is proposed that the [3Fe-4S] cluster plays a vital role in this activation and that [NiFe]-hydrogenases without such a cluster probably use a different reaction route for activation.

(3) Oxygen delays the reaction of ready enzyme with H_2, but it does not prevent it. In the presence of hydrogen, ready enzyme reduces oxygen with a rate of ca. 0.03 s^{-1}.

While not yet providing a complete kinetically defined mechanism of hydrogenase activation, we consider the present and accompanying paper (*30*) to significantly increase our understanding of these complex processes and demonstrate the considerable potential of the new technique of anaerobic stopped-flow FTIR spectroscopy for hydrogenase research.

REFERENCES

1. Cammack, R., Frey, M., and Robson, R. (2001) *Hydrogen as a fuel. Learning from Nature*, Taylor & Francis Inc, New York.
2. Adams, M. W. (1990) The structure and mechanism of iron−hydrogenases, *Biochim. Biophys. Acta 1020*, 115−145.
3. Albracht, S. P. J. (1994) Nickel hydrogenases: in search of the active site, *Biochim. Biophys. Acta 1188*, 167−204.
4. Vignais, P. M., Billoud, B., and Meyer, J. (2001) Classification and phylogeny of hydrogenases, *FEMS Microbiol. Rev. 25*, 455−501.
5. Zirngibl, C., Hedderich, R., and Thauer, R. K. (1990) N^5, N^{10}-Methylenetetrahydromethanopterin dehydrogenase from *Methanobacterium thermoautotrophicum* has hydrogenase activity, *FEBS Lett. 261*, 112−116.
6. Afting, C., Hochheimer, A., and Thauer, R. K. (1998) Function of H_2-forming methylenetetrahydromethanopterin dehydrogenase from *Methanobacterium thermoautotrophicum* in coenzyme F_{420} reduction with H_2, *Arch. Microbiol. 169*, 206−210.
7. Lyon, E. J., Shima, S., Buurman, G., Chowdhuri, S., Batschauer, A., Steinbach, K., and Thauer, R. K. (2004) UV-A/blue-light inactivation of the 'metal-free' hydrogenase (Hmd) from methanogenic archaea, *Eur. J. Biochem. 271*, 195−204.
8. Volbeda, A., Charon, M. H., Piras, C., Hatchikian, E. C., Frey, M., and Fontecilla-Camps, J. C. (1995) Crystal structure of the nickel−iron hydrogenase from *Desulfovibrio gigas*, *Nature 373*, 580−587.
9. Volbeda, A., Garcia, E., Piras, C., deLacey, A. L., Fernandez, V. M., Hatchikian, E. C., Frey, M., and Fontecilla-Camps, J. C. (1996) Structure of the [NiFe] hydrogenase active site: Evidence for biologically uncommon Fe ligands, *J. Am. Chem. Soc. 118*, 12989−12996.
10. Montet, Y., Amara, P., Volbeda, A., Vernede, X., Hatchikian, E. C., Field, M. J., Frey, M., and Fontecilla-Camps, J. C. (1997) Gas access to the active site of Ni−Fe hydrogenases probed by X-ray crystallography and molecular dynamics, *Nat. Struct. Biol. 4*, 523−526.
11. Higuchi, Y., Yagi, T., and Yasuoka, N. (1997) Unusual ligand structure in Ni−Fe active center and an additional Mg site in hydrogenase revealed by high-resolution X-ray structure analysis, *Structure 5*, 1671−1680.
12. Higuchi, Y., Ogata, H., Miki, K., Yasuoka, N., and Yagi, T. (1999) Removal of the bridging ligand atom at the Ni−Fe active site of [NiFe] hydrogenase upon reduction with H_2, as revealed by X-ray structure analysis at 1.4 angstrom resolution, *Struct. Folding Des. 7*, 549−556.
13. Garcin, E., Vernede, X., Hatchikian, E. C., Volbeda, A., Frey, M., and Fontecilla-Camps, J. C. (1999) The crystal structure of a reduced [NiFeSe] hydrogenase provides an image of the activated catalytic center, *Struct. Folding Des. 7*, 557−566.
14. Matias, P. M., Soares, C. M., Saraiva, L. M., Coelho, R., Morais, J., Le Gall, J., and Carrondo, M. A. (2001) [NiFe] hydrogenase from *Desulfovibrio desulfuricans* ATCC 27774: gene sequencing, three-dimensional structure determination and refinement at 1.8 Å and modelling studies of its interaction with the tetrahaem cytochrome c3, *J. Biol. Inorg. Chem. 6*, 63−81.
15. Ogata, H., Mizoguchi, Y., Mizuno, N., Miki, K., Adachi, S., Yasuoka, N., Yagi, T., Yamauchi, O., Hirota, S., and Higuchi, Y. (2002) Structural studies of the carbon monoxide complex of [NiFe]hydrogenase from *Desulfovibrio vulgaris* Miyazaki F: suggestion for the initial activation site for dihydrogen, *J. Am. Chem. Soc. 124*, 11628−11635.
16. Volbeda, A., Montet, Y., Vernède, X., Hatchikian, E. C., and Fontecilla-Camps, J. C. (2002) High-resolution crystallographic analysis of *Desulfovibrio fructosovorans* [NiFe] hydrogenase, *Int. J. Hydr. Energy 27*, 1449−1461.
17. Bagley, K. A., Duin, E. C., Roseboom, W., Albracht, S. P. J., and Woodruff, W. H. (1995) Infrared-detectable groups sense changes in charge density on the nickel center in hydrogenase from *Chromatium vinosum*, *Biochemistry 34*, 5527−5535.
18. Happe, R. P., Roseboom, W., Pierik, A. J., Albracht, S. P. J., and Bagley, K. A. (1997) Biological activation of hydrogen, *Nature 385*, 126.
19. Pierik, A. J., Roseboom, W., Happe, R. P., Bagley, K. A., and Albracht, S. P. J. (1999) Carbon monoxide and cyanide as intrinsic ligands to iron in the active site of [NiFe]-hydrogenases. NiFe-$(CN)_2CO$, Biology's way to activate H_2, *J. Biol. Chem. 274*, 3331−3337.
20. Van der Spek, T. M., Arendsen, A. F., Happe, R. P., Yun, S., Bagley, K. A., Stufkens, D. J., Hagen, W. R., and Albracht, S. P. J. (1996) Similarities in the architecture of the active sites of Ni-hydrogenases and Fe-hydrogenases detected by means of infrared spectroscopy, *Eur. J. Biochem. 237*, 629−634.
21. De Lacey, A. L., Hatchikian, E. C., Volbeda, A., Frey, M., Fontecilla-Camps, J. C., and Fernandez, V. M. (1997) Infrared

spectroelectrochemical characterization of the [NiFe] hydrogenase of *Desulfovibrio gigas*, *J. Am. Chem. Soc. 119*, 7181−7189.
22. Surerus, K. K., Chen, M., van der Zwaan, J. W., Rusnak, F. M., Kolk, M., Duin, E. C., Albracht, S. P. J., and Münck, E. (1994) Further characterization of the spin coupling observed in oxidized hydrogenase from *Chromatium vinosum*. A Mössbauer and multifrequency EPR study, *Biochemistry 33*, 4980−4993.
23. Gu, Z. J., Dong, J., Allan, C. B., Choudhury, S. B., Franco, R., Moura, J. J. G., LeGall, J., Przybyla, A. E., Roseboom, W., Albracht, S. P. J., Axley, M. J., Scott, R. A., and Maroney, M. J. (1996) Structure of the Ni sites in hydrogenases by X-ray absorption spectroscopy. Species variation and the effects of redox poise, *J. Am. Chem. Soc. 118*, 11155−11165.
24. Davidson, G., Choudhury, S. B., Gu, Z., Bose, K., Roseboom, W., Albracht, S. P. J., and Maroney, M. J. (2000) Structural examination of the nickel site in *Chromatium vinosum* hydrogenase: redox state oscillations and structural changes accompanying reductive activation and CO binding, *Biochemistry 39*, 7468−7479.
25. Huyett, J. E., Carepo, M., Pamplona, A., Franco, R., Moura, I., Moura, J. J. G., and Hoffman, B. M. (1997) Fe-57 Q-band pulsed ENDOR of the hetero-dinuclear site of nickel hydrogenase: Comparison of the NiA, NiB, and NiC states, *J. Am. Chem. Soc. 119*, 9291−9292.
26. George, S. J., Ashby, G. A., Wharton, C. W., and Thorneley, R. N. F. (1997) Time-resolved binding of carbon monoxide to nitrogenase monitored by stopped-flow infrared spectroscopy, *J. Am. Chem. Soc. 119*, 6450−6451.
27. Thorneley, R. N. F., and George, S. J. (2000) Time-resolved infrared spectroscopy of functioning nitrogenase, in *Nitrogen Fixation in Bacteria: Cellular and Molecular Biology* (Triplett, E., Ed.) pp 81−99, Horizon Scientific Press, Wymondham, UK.
28. Muthusamy, M., Ambundo, E. A., George, S. J., Lippard, S. J., and Thorneley, R. N. F. (2003) Stopped-Flow Fourier Transform Infrared Spectroscopy of Nitromethane Oxidation by the Diiron(IV) Intermediate of Methane Monooxygenase, *J. Am. Chem. Soc. 125*, 11150−11151.
29. Coremans, J. M. C. C., van der Zwaan, J. W., and Albracht, S. P. J. (1992) Distinct redox behaviour of prosthetic groups in ready and unready hydrogenase from *Chromatium vinosum*, *Biochim. Biophys. Acta 1119*, 157−168.
30. George, S. J., Kurkin, S., Thorneley, R. N. F., and Albracht, S. P. J. (2004) Reactions of H_2, CO and O_2 with active [NiFe]-hydrogenase from *Allochromatium vinosum*. A stopped-flow infrared study, *Biochemistry 43*, 6808−6819.
31. Bradford, M. M. (1976) A rapid and sensitive method for the quantitation of microgram quantities of protein utilising the principle of protein-dye binding, *Anal. Biochem. 100*, 201−220.
32. Bleijlevens, B., Faber, B. W., and Albracht, S. P. J. (2001) The [NiFe] hydrogenase from *Allochromatium vinosum* studied in EPR-detectable states: H/D exchange experiments that yield new information about the structure of the active site, *J. Biol. Inorg. Chem. 6*, 763−769.
33. White, A. J., Drabble, K., and Wharton, C. W. (1995) A stopped-flow apparatus for infrared-spectroscopy of aqueous-solutions, *Biochem. J. 306*, 843−849.
34. George, S. J., Allen, J. W. A., Ferguson, S. J., and Thorneley, R. N. F. (2000) Time-resolved infrared spectroscopy reveals a stable ferric heme-NO intermediate in the reaction of *Paracoccus pantotrophus* cytochrome *cd1* nitrite reductase with nitrite, *J. Biol. Chem. 275*, 33231−33237.
35. Kurkin, S., Meuer, J., Koch, J., Hedderich, R., and Albracht, S. P. J. (2002) The membrane-bound [NiFe]-hydrogenase (Ech) from *Methanosarcina barkeri*: unusual properties of the iron-sulphur clusters, *Eur. J. Biochem. 269*, 6101−6111.
36. Fernandez, V. M., Hatchikian, E. C., and Cammack, R. (1985) Properties and reactivation of two different deactivated forms of *Desulfovibrio gigas* hydrogenase, *Biochim. Biophys. Acta 832*, 69−79.
37. Fernandez, V. M., Rao, K. K., Fernandez, M. A., and Cammack, R. (1986) Activation and deactivation of the membrane-bound hydrogenase from *Desulfovibrio desulfuricans*, Norway strain, *Biochimie 68*, 43−48.
38. van der Zwaan, J. W., Coremans, J. M. C. C., Bouwens, E. C., and Albracht, S. P. J. (1990) Effect of $^{17}O_2$ and ^{13}CO on EPR spectra of nickel in hydrogenase from *Chromatium vinosum*, *Biochim. Biophys. Acta 1041*, 101−110.
39. Cammack, R., Patil, D., Aquirre, R., and Hatchikian, E. C. (1982) Redox properties of the esr-detectable nickel in hydrogenase from *Desulfovibrio gigas*, *FEBS Lett. 142*, 289−292.
40. Teixeira, M., Moura, I., Xavier, A. V., Moura, J. J. G., LeGall, J., DerVartanian, D. V., Peck, H. D., Jr., and Huynh, B. H. (1989) Redox intermediates of *Desulfovibrio gigas* [NiFe] hydrogenase generated under hydrogen. Mössbauer and EPR characterization of the metal centers, *J. Biol. Chem. 264*, 16435−16450.
41. Bleijlevens, B. (2002) Activation and sensing of hydrogen in nature, Ph.D. Thesis, University of Amsterdam, Amsterdam.
42. Bagley, K. A., Van Garderen, C. J., Chen, M., Duin, E. C., Albracht, S. P. J., and Woodruff, W. H. (1994) Infrared studies on the interaction of carbon monoxide with divalent nickel in hydrogenase from *Chromatium vinosum*, *Biochemistry 33*, 9229−9236.
43. Bleijlevens, B. (2001) The hydrogen-consumption activity of the [NiFe] hydrogenase of *Allochromatium vinosum* in different redox states, in *Hydrogen as a Fuel. Learning from Nature* (Cammack, R., Frey, M., and Robson, R., Eds.) pp 82−84, Taylor & Francis, London.
44. Van der Zwaan, J. W., Albracht, S. P. J., Fontijn, R. D., and Slater, E. C. (1985) Monovalent nickel in hydrogenase from *Chromatium vinosum*. Light sensitivity and evidence for direct interaction with hydrogen, *FEBS Lett. 179*, 271−277.
45. Coremans, J. M. C. C., van Garderen, C. J., and Albracht, S. P. J. (1992) On the redox equilibrium between H_2 and hydrogenase, *Biochim. Biophys. Acta 1119*, 148−156.
46. Barondeau, D. P., Roberts, L. M., and Lindahl, P. A. (1994) Stability of the Ni−C state and oxidative titrations of *Desulfovibrio-gigas* hydrogenase monitored by EPR and electronic absorption spectroscopies, *J. Am. Chem. Soc. 116*, 3442−3448.
47. Cammack, R., Patil, D. S., Hatchikian, E. C., and Fernández, V. M. (1987) Nickel and iron-sulphur centres in *Desulfovibrio gigas* hydrogenase: ESR spectra, redox properties and interactions, *Biochim. Biophys. Acta 912*, 98−109.
48. Foerster, S., Stein, M., Brecht, M., Ogata, H., Higuchi, Y., and Lubitz, W. (2003) Single-crystal EPR studies of the reduced active site of [NiFe] hydrogenase from *Desulfovibrio vulgaris* Miyazaki F, *J. Am. Chem. Soc. 125*, 83−93.
49. Brecht, M., van Gastel, M., Buhrke, T., Friedrich, B., and Lubitz, W. (2003) Direct detection of a hydrogen ligand in the [NiFe] center of the regulatory H_2-sensing hydrogenase from *Ralstonia eutropha* in its reduced state by HYSCORE and ENDOR spectroscopy, *J. Am. Chem. Soc. 125*, 13075−13083.
50. Tran-Betcke, A., Warnecke, U., Bocker, C., Zaborosch, C., and Friedrich, B. (1990) Cloning and nucleotide sequences of the genes for the subunits of NAD-reducing hydrogenase of *Alcaligenes eutrophus* H16, *J. Bacteriol. 172*, 2920−2929.
51. Jones, A. K., Lamle, S. E., Pershad, H. R., Vincent, K. A., Albracht, S. P. J., and Armstrong, F. A. (2003) Enzyme electrokinetics: electrochemical studies of the anaerobic interconversions between active and inactive states of *Allochromatium vinosum* [NiFe]-hydrogenase, *J. Am. Chem. Soc. 125*, 8505−8514.

BI049854C